Tribological investigation of truncated thermo-elastohydrodynamic elliptical point contacts in high performance transmissions

3rd Biennial International Conference on Powertrain Modelling and Control (PMC 2016)
Testing, Mapping and Calibration
7th-9th September 2016, Loughborough University, UK

Tribological Investigation of Truncated thermo-Elastohydrodynamic Elliptical Point Contacts in High Performance Transmissions

V. Elisaus, M. Mohammadpour, S. Theodossiades and H. Rahnejat

Wolfson School of Mechanical, Electrical and Manufacturing Engineering, Loughborough University, Loughborough, Leicestershire, UK

Abstract:

In high performance cars, light-weighting is a major development driver. Consequently, the transmission can be particularly compact whilst being subject to large variations in torque and power. Pitch line velocities of up to 52 m/s and contact pressures of up to 3 GPa are routinely encountered under race conditions.

Contact patch asymmetry due to angular misalignments between input and output shafts leads to the generation of high contact edge pressures, with the potential of inducing fatigue spalling, which can be exacerbated by observed and yet unexplained contact footprint truncation. Crowning is widely used as a palliative measure for these undesired conditions. The paper provides a time-efficient analytical method to solve the non-Newtonian mixed thermo-elastohydrodynamic (TEHD) problem under the extreme prevalent conditions in such high performance vehicle transmission systems. The approach expounded in this paper for the extreme tribological conditions has not hitherto been reported in literature.

Keywords: *High performance transmissions, Spur Gear, thermo-elastohydrodynamics, Non-Newtonian traction*

1-Introduction

The modern light-weight and compact concept in vehicle systems provides significant advantages in terms of drivability and fuel efficiency, but can lead to a plethora of noise and vibration concerns. Weight reduction of rotational components in the driveline in particular, desirably improves throttle response and errant rigid body dynamics, however often at the expense of vibration and noise from hollow driveshaft tubes [1]. In transmissions, gear shafts can be made hollow to be in line with the light-weight concept. This is particularly true of transmissions of high performance cars. Shaft-integrated lubricant galleries can also be present to lubricate the bearing supports and gear contact conjunctions, but require the removal of additional material which further adds to the reduction in component rigidity. Short and stubby

gear shafts and appropriate material selection mitigate elastodynamic behaviour to a large extent and whilst shaft components still remain considerably stiff, contact loads at gear teeth meshing conjunctions in high performance cars can routinely exceed 20 kN. The combined deflection that results from the compliance of load bearing components has been found to cause sufficient relative angular displacement between the shafts to result in edge loading of teeth pair contact patches as well as cause asymmetrical loading on the mating flanks. Inspection of gears run in situ has shown skewed scuffing due to the uneven stress distribution across the gear teeth flanks caused by misalignment. This has led to the use of teeth crowning as a palliative measure. At sufficiently high loads, any minor curvature of the flank, induced along the semi-major axis of the elliptical contact footprint through the application of crowning, is essentially 'flattened' due to the deformation of the solid surfaces. With particularly compact gears, such as in the transmissions of high performance cars, this can routinely cause truncation of the contact ellipse which would in turn likely cause areas of highly localized pressures on the flank edges. This is caused by stress discontinuities resulting from the abrupt change in profile, similar to those at the edges of rolling element bearings and the relief of the same through crowning [2-4]. The resulting contact footprint shape is that of a truncated finite line contact and not an elliptical one.

Several authors have investigated the improvements in the meshing contact distribution of misaligned spur gears through crowning [5-7]. However, these primarily focused on mitigating the effects of misalignment on maldistribution of load along the flank without regard to truncation of the contact ellipse footprint and its effect on incurred frictional losses. Harianto and Houser [8] assessed crowning and its induced variation in stress distribution within an active area of the face-width. Variations in peak-to-peak transmission error were also presented by varying the amount of crowning and misalignment to assess their implications on gear dynamics. A similar analysis was conducted by Seol and Kim [9], where the effect of crowning on dynamic transmission error and the dynamic loading factor were assessed. While truncation was observed in the results presented by Mao [5], no further assessment seems to have been conducted to establish whether the occurrence of truncation is a hindrance to transmission efficiency.

This paper provides a time-efficient solution of non-Newtonian mixed thermo-elastohydrodynamics of gear teeth meshing combined with a thermal partitioning method to determine the flash temperature of the mating surfaces. It predicts the generated friction due to

non-Newtonian viscous shear of a thin film as well as boundary friction due to interaction of asperities on the opposing contact surfaces. Conditions promoting contact footprint truncation are identified as well as the effects of crowning and the extent of its influence on transmission efficiency and power loss.

2- Method of Analysis

2.1- Lubricated contacts

During operation, loaded gear teeth routinely experience contact pressures in the order of 1-3 GPa. The meshing conjunction operates under Elastohydrodynamic (EHD) lubrication with Newtonian or non-Newtonian shear of the lubricant film, depending on the prevailing contact conditions; contact kinematics and load [10-13]. Contact friction in EHD conjunctions comprises of the viscous shear of a thin lubricant film and any direct interaction between the surfaces of meshing teeth pairs. For an analytical solution, such as that in [10], estimation of lubricant film thickness is crucial in determining the regime of lubrication. This can be performed through use of lubricant film thickness equations, originally provided by Ertel and Grubin [14]. Subsequently, many authors have provided similar expressions through regression of many numerical results at different combinations of operating conditions, such as contact speed and load [15-18]. A comprehensive list of these earlier equations is provided in [19]. All these equations were for steady state conditions and did not include features such as squeeze film effect in mutual approach of surfaces or changes in the lubricant entrainment angle into the contact as the result of rolling and sliding. For the former, Jalali-Vahid et al [20] provided an equation, verified by optical interferometric studies, and Rahnejat [21] provided a squeeze film term in addition to Mostofi and Gohar's [22] generalised elliptical point contact with angles entrainment flow, an approach which was also made by Chittenden et al [23]. Similar expressions exist for finite line contact footprints [24]. However, the current study assumes an elliptical point contact footprint of large aspect ratio, thus the expression in [23] is used:

$$h_c = 4.31 R_x U_e^{0.68} G_e^{0.49} W_e^{-0.073} \left\{1 - exp\left[-1.23 \left(\frac{R_y}{R_x}\right)^{2/3}\right]\right\} \quad (1)$$

Where, the non-dimensional groups are:

$$W_e = \frac{\pi W}{2 E_r R_x^2},\ U_e = \frac{\pi \eta_0 U_r}{4 E_r R_x},\ G_e = \frac{2}{\pi}(E_r \alpha)$$

where W is the instantaneous total normal contact load, E_r is the reduced elastic modulus of contact, R_x and R_y are the equivalent principal contact radii of curvature along the lubricant entrainment (minor axis) and side leakage directions (semi-major axis) respectively, η_0 is the lubricant viscosity, U_r is the is speed of entrainment, α is the lubricant pressure-viscosity coefficient, and h_c is the central film thickness.

Due to the limitations in computational power, early solutions assumed low to medium contact loads with fully flooded inlets and isothermal Newtonian conditions. Most gearing contact inlets are starved as some of the inlet flow is subjected to counter and swirl flows. Therefore, zero reverse flow boundary should be determined, beyond which all the entrained lubricant is drawn into the contact as determined by Tipei [25] and shown experimentally by Johns-Rahnejat and Gohar [26] and numerically by Mohammadpour et al [27]. Inlet starvation reduces the contact film thickness, thus affecting friction and power loss. This approach assumes a fully flooded inlet, which is the basis of equation (1) and film thickness is assumed not to vary along the semi-major axis which significantly reduces computation time.

2.2- Tooth Contact Analysis

EHL formulations used for the prediction of the lubricant film thickness as in (1) require prior knowledge equivalent contact curvature of meshing contact, as well as the instantaneous surface velocities of the two teeth surfaces. This serves to estimate the speed of lubricant entrainment and sliding velocity. These parameters are obtained through tooth contact analysis [28].

Through the application of a finite element technique, the Tooth Contact Analysis (TCA) software (CALYX, Advanced Numerical Solutions) employed in this study allows for accurate representation of contact geometry and the estimation of contact curvature and kinematics for a set of loaded, modified spur gear teeth. Although classical methods of gear contact analysis that consider involute geometry are faster and computationally more efficient, they do not take into account the effects more intricate three-dimensional tooth modifications such as crowning.

The contact load applied per teeth pair is a function of the dynamic response of the system. The ratio of the applied load W_i on a given flank under consideration to the total transmitted load W_T [11] is known as the load factor, lf is a function of the pinion angle. Therefore, the load per pair of contacting teeth pair is obtained as:

$$lf = \frac{W}{W_T} \tag{2}$$

where, the total load on the gear pair is obtained from the applied torque.

Time varying contact stiffness's resulting from the variation in meshing contact location and simultaneous load sharing between multiple teeth pairs is taken into account through TCA to acquire representative individual tooth loading distributions.

The speed of lubricant entraining motion, U_r for use in equation (1) at any instant of time during a gear teeth pair meshing cycle. to be used in (4). The velocity of any point on the pinion and gear teeth in contact may be obtained as:

$$v_p = \omega_p(n_p \times R_p), and\ v_g = \omega_g(n_g \times R_g) \tag{3}$$

where, n_p and n_g are the unit vectors along the pinion and gear axes, respectively. R_p and R_g are the position vectors of the contact point with respect to the coordinate system attached to the axes of the pinion and gear, respectively. These velocities can be resolved along the normal direction (v_p^n and v_g^n) and along the tangential plane ($v_p^t\ and\ v_g^t$). The tangential components are used to obtain the rolling and sliding contact velocities. These components, as well as those along the major and minor axes of the Hertzian contact ellipse can be presented using vector dot products:

$$v_p^{t,major} = v_p \bullet n_{major}, v_g^{t,major} = v_g \bullet n_{major}, v_p^{t,minor} = v_p \bullet n_{minor}, v_p^{t,minor} = v_p \bullet n_{minor} \tag{4}$$

where, $v_p^{t,major}$ and $v_p^{t,minor}$ are the components of the pinion surface velocities along the major and minor axis and, n_{major} and n_{minor} are the unit vectors of the major and minor axis.

Therefore, for entraining velocity along the minor axis of the elliptical contact footprint, as in the case of spur gears:

$$U_r = \frac{1}{2}\left(v_p^{t,minor} + v_g^{t,minor}\right) \tag{5}$$

And note that with no side-leakage: $v_p^{t,major} = v_g^{t,major} = V = 0$

As TCA is sensitive to variation in contact geometry along the flank, position vectors that take into local deformation on crowned flanks are obtained to calculate variation in kinematic parameters at discrete locations along the major axis of the prevailing contact patch.

To observe the crowning induced variations in localized contact pressures along the semi-major axis of the elliptical footprint, the instantaneous contact ellipse is discretised into a number of finite equivalent rectangular strips (similar to the contact of slender cylindrical rollers). The semi-major and semi-minor half-widths of the prevailing contact ellipse, a and b can be calculated as [18]:

$$a = \left(\frac{6\bar{k}^2\bar{\varepsilon}WR'}{\pi E'}\right)^{1/3} \tag{6}$$

$$b = \left(\frac{6\bar{\varepsilon}WR'}{\pi\bar{k}E'}\right)^{1/3} \tag{7}$$

where, R' is the reduced contact radii of curvature, E' is the reduced elastic modulus, $\bar{k}$ is the ellipticity parameter given by:

$$\bar{k} = 1.0339 + \left(\frac{R_y}{R_x}\right)^{0.636}$$

And:

$$\bar{\varepsilon} = 1.0003 + \frac{0.5968R_x}{R_y}$$

The resulting contact ellipse is discretized into n individual rectangular contact strips, where the semi-major and semi-minor half-widths of each strip, a_j and b_j are:

$$a_j = \frac{a}{n}\ where\ j = 1,2,3 \ldots n \tag{8}$$

$$b_j = \left(\frac{4WR'}{\pi a_j E'}\right)^{1/2} \tag{9}$$

and the contact area of each strip is:

$$A_j = 4a_j b_j \tag{10}$$

The distance of the centre-point of a strip j from the centre-point of the contact ellipse along the semi-major axis is:

$$x_j = -a + \left(\frac{2a}{n}(j-1)\right) + a_j \tag{11}$$

For instances where the contact ellipse is truncated at the gear teeth flank edges, the total length of the contact semi-major axis is limited to the length of the gear flank t. The semi-major axis of each individual discretized strip then becomes:

$$a_j = \frac{\frac{t}{2}}{n} \tag{12}$$

and x_j is given by:

$$x_j = -\frac{t}{2} + \left(\frac{t}{n}(j-1)\right) + a_j \tag{13}$$

The local load acting over each discretized strip W_j is estimated using knowledge of the load intensity distribution $Q(x)$ acquired through TCA, as illustrated in Fig. 1.

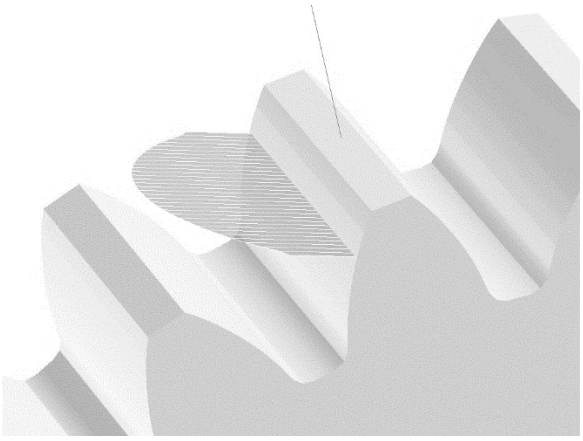

Figure 1: Instantaneous flank load intensity distribution - TCA

$$W_j = \int_{x-a}^{x+a} Q(x) \tag{14}$$

where, the average contact pressure acting at each discretized strip becomes:

$$\bar{p}_j = \frac{W_j}{A_j} \tag{15}$$

2.3- Viscous friction

The conditions investigated in the current analysis pertains to transmissions of high performance vehicles at high contacts loads and shear rates, leading to thin TEHD conditions with non-Newtonian shear of the lubricant film. Evans and Johnson [29] modified Crook's [30] original thermal analysis of Newtonian fluids to account for discrepancies between theoretical and observed values of viscous traction in EHD contacts. They provided an analytical expression for coefficient of friction under TEHD conditions subject to non-Newtonian shear of a thin film, which is utilised in this analysis [29]:

$$\mu_j = 0.87\alpha\tau_0 + 1.74\frac{\tau_0}{\bar{p}_j} ln\left[\frac{1.2}{\tau_0 h_c}\left(\frac{2K\eta_0}{1+9.6\xi_j}\right)^{\frac{1}{2}}\right] \tag{16}$$

Note that the coefficient of friction is calculated for each discretise strip of the instantaneous contact. Therefore, an average of these can represent the value at any instant of time during the meshing cycle. τ_0 is the lubricant Eyring stress, K its thermal conductivity, and ξ_j is:

$$\xi_j = \frac{4}{\pi}\frac{K}{h_c/R_{x,j}}\left(\frac{\bar{p}_j}{E'R_{x,j}K'\rho'c'U_{r,j}}\right)^{1/2} \tag{17}$$

where, $R_{x,j}$ is the local reduced contact radius of curvature in the direction of lubricant entrainment at position x_j, and K', ρ', and c' are the thermal conductivity, density, and specific heat capacity of the solids respectively.

The generated friction due to viscous shear of the lubricant film is then expressed as

$$f_{v,j} = \mu_j W_j \tag{18}$$

2.4- Flash surface contact temperature

Crook [30] showed that heat generated due to viscous friction is transferred across the film through conduction to the solid surfaces, which in turn rapidly convects away. Through the reasonable assumption that the shear stress τ varied parabolically along the direction of lubricant entrainment, Crook showed that the temperature rise of the solid surfaces in the EHD conjunction, from bulk temperature θ_O, is given by

$$\theta_{s,j} - \theta_{O,j} = + \frac{0.5 T_j \Delta U_j}{\left(\pi K' \rho' c' b_j \bar{U}_j\right)^{1/2}} \tag{19}$$

where, T is the traction per unit width given by:

$$T_j = \frac{2 b_j f_{v,j}}{A_j} \tag{20}$$

ΔU is the sliding velocity, and $\bar{U}$ is the rolling velocity.

With the assumption that heat generation occurs locally at the centre-plane of the lubricant film and that the separated solid surfaces are at equal temperatures, Johnson and Greenwood [31] derived formulae estimating the temperature rise across the lubricant film. The resulting estimate is the local temperature rise averaged across the semi-minor axis of the elliptical contact footprint at any instant of time. With the assumption that the lubricant thermal conductivity remains constant, whilst its dynamic viscosity reduces exponentially with the temperature rise and the lubricant's temperature-viscosity coefficient β, they were able to accurately predict the prevailing lubricant film centre-plane temperature as:

$$\frac{T_j \Delta U_j h_c \beta_L}{16 b_j K} = \frac{(1 + {X_j}^2)^{1/2}}{X_j \sinh^{-1} X_j} \tag{21}$$

$$X_j = \sqrt{e^{\beta(\theta_{c,j} - \theta_{s,j})} - 1} \tag{22}$$

The work in [31] further led to the derivation of equation (16) of Evans and Johnson [29] presented in section 2.3. While these formulations serve to predict the temperature at the centre plane of the contact, it is merely used to observe temperature variation on the active teeth flank area. Thermal predictions do not serve to vary rheological parameters (provided in Table 2) during the course of the simulation as they may do so in reality.

2.5- Boundary Friction

The thin lubricant films in the meshing contacts of loaded gear teeth pairs in high performance transmissions are comparable in magnitude to the roughness of the teeth flanks. Consequently, asperity interaction and therefore boundary friction is to be expected. Figure 2 is an image of a patch of a tooth flank obtained through use of white light interferometry with a vertical

resolution (in the *z*-direction) of 10 nm and 0.175 μm in the contacting *xy* plane. The gear considered has been subjected to severe race conditions for a distance of 4000 km, well past its run-in state.

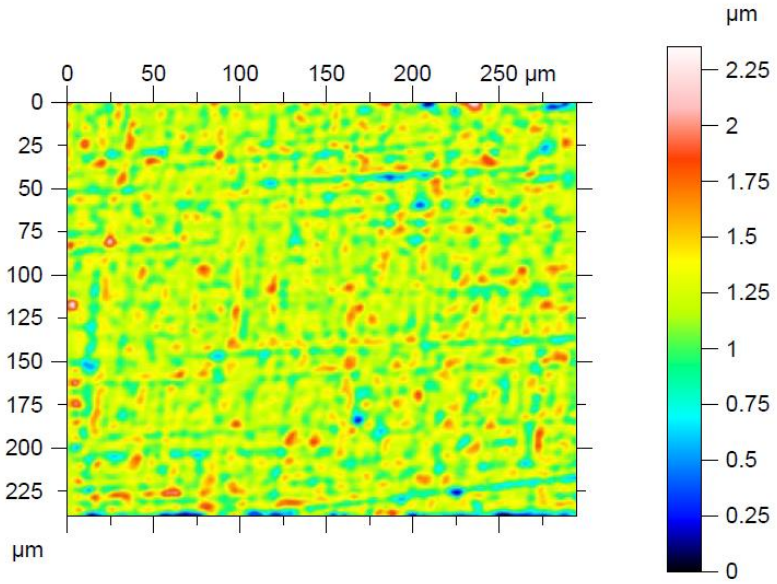

Figure 2: Surface Roughness of gear tooth flank centre after 4000km on a high performance racing drive cycle

Greenwood and Tripp [32] developed a method to evaluate the generated boundary friction as the result of direct interaction of asperities on the counter face contacting surfaces. The method assumes a Gaussian height distribution of surface asperities. When mixed or boundary regimes of lubrication occur, Stribeck's oil film parameter: $1 < \lambda = \frac{h_c}{\sigma} < 2.5$, specifies the fraction of the load carried by the asperities in each discretized contact area, A_j as:

$$W_{a,j} = \frac{16\sqrt{2}}{15}\pi(\xi\beta\sigma)^2\sqrt{\frac{\sigma}{\beta}}E'A_jF_{5/2}(\lambda) \tag{23}$$

where, β is the average asperity tip radius, σ is the composite RMS surface roughness of the contacting surfaces, and the statistical function F5/2(λ) for a Gaussian distribution of asperities can be represented by a polynomial fit function as [33]:

$$F_{5/2} = \begin{cases} -0.004\lambda^5 - 0.057\lambda^4 - 0.29\lambda^3 - 0.784\lambda^2 - 0.784\lambda - 0.617 & \text{for } \lambda < 2.5 \\ 0; & \text{for } \lambda \geq 2.5 \end{cases} \tag{24}$$

The roughness parameter $(\xi\beta\sigma)$ for steel surfaces is generally in the range of 0.01–0.07 [33]. The average asperity slope (σ/β) and is in the range of 10^{-4}-10^{-2} [24]. Surface measurements

of the load bearing flank centre of the gear considered in this study, using focus variation imaging yielded $\xi\beta\sigma$ = 0.011 and σ/β = 0.0194.

Asperity friction should be considered in mixed and boundary regimes of lubrication. A thin adsorbed film exists at the summit of the asperities or is entrapped in their inter-spatial valleys. This thin adsorbed film is subjected to non-Newtonian shear, thus boundary friction $f_{b,j}$ at each discretised strip is given by as:

$$f_{b,j} = \tau_L A_{a,j} \tag{25}$$

where, the asperity contact area $A_{a,j}$ [32] is:

$$A_{a,j} = \pi^2(\xi\beta\sigma)^2 A_j F_2(\lambda) \tag{26}$$

and the lubricant's limiting shear stress τ_L given by [34]:

$$\tau_{L,j} = \tau_0 + \varepsilon P_{m,j} \tag{27}$$

where, ε is the slope of the lubricant limiting shear stress-pressure dependence, and the mean pressure $P_{m,j}$ is:

$$P_{m,j} = \frac{W_{a,j}}{A_{a,j}} \tag{28}$$

and the statistical function F2(λ) expressed as [33]:

$$F_2(\lambda) = \begin{cases} -0.002\lambda^5 - 0.028\lambda^4 - 0.173\lambda^3 + 0.526\lambda^2 - 0.804\lambda - 0.500 & for\ \lambda < 2.5 \\ 0; & for\ \lambda \geq 2.5 \end{cases} \tag{29}$$

In this study, the topographical properties of the contacting teeth surfaces (i.e. surface roughness, roughness parameter, and average asperity slope) are assumed constant both along and across the flank. However, values used in this study are based on measurements sampled over multiple areas of the flank, thus it is unlikely to significantly affect the results of the analysis.

2.6- Power Loss

The total instantaneous friction in each discretised element is as the combined results of viscous and boundary friction contributions:

$$f_{T,j} = f_{v,j} + f_{b,j} \tag{30}$$

The instantaneous power loss per instantaneous contact strip is determined as:

$$P_{loss,j} = f_{T,j} U_{s,j} \tag{31}$$

where, $U_{s,j}$ is the local sliding velocity, acting at the centre of the discretised contact strip, j.

3-Results and Discussion

The effects of symmetric crowning as illustrated in Figure 3, and contact ellipse truncation on contact efficiency in spur gears is studied.

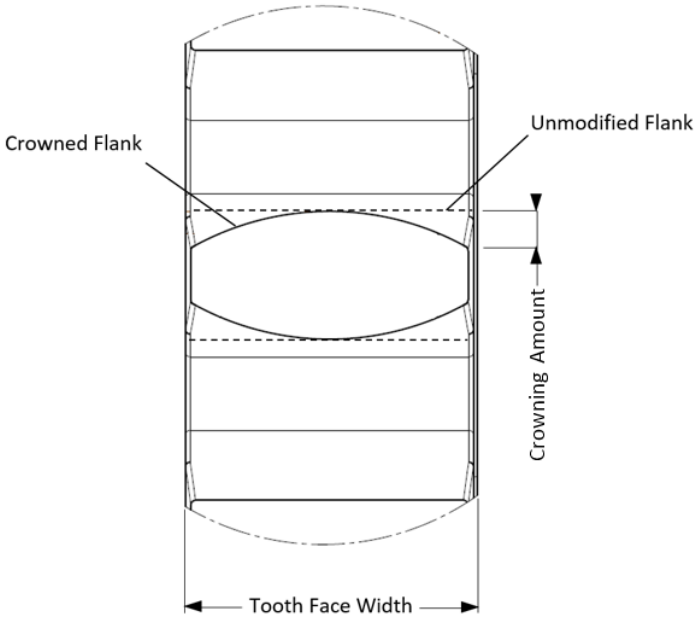

Figure 3: Symmetric Gear teeth crowning modification (plan view)

The simulated conditions are typical of high performance transmissions and are given in Table 1, along with relevant design parameters of the gear pair assessed and the operating conditions.

Table 1: Pinion and gear parameters

Module (mm)	3.6
Number of teeth (pinion:gear)	27:27
Pitch diameter (pinion:gear) (mm)	97:97
Normal pressure angle (°)	25
Face width (mm)	13.5

Pinion speed (RPM)	9500
Pinion torque (Nm)	700
Bulk solid temperature (°C)	130

Table 2 lists the relevant data for solid surfaces and the lubricant rheological properties.

Table 2: Lubricant rheology and surface data

Pressure viscosity coefficient (Pa-1)	1.05×10^{-8}
Lubricant dynamic viscosity at atmospheric pressure at 130°C (mPa.s)	4.04
Lubricant Eyring stress (MPa)	2
Thermal conductivity of fluid (W/mK)	0.137
Modulus of elasticity of contacting solid (GPa)	206
Poisson's ratio of contacting solids (–)	0.3
Density of contacting solids (kg/m3)	7800
Thermal conductivity of contacting solids (W/m.K)	46.7
Heat capacity of contacting solids (J/kg K)	460
RMS composite Surface roughness (µm)	0.2
Roughness parameter ($\xi\beta\sigma$)	0.011
Average asperity slope (σ/β)	0.0194

Table 3 lists the amount of crowning applied for each studied scenario. All crowning assessed is symmetric.

Table 3: Amount of crowning and semi-major axis curvatures

Scenario	Crowning Amount (µm)	Contact radii of curvature (along semi-major axis) (m)
A	2.5	9.12
B	5	4.56
C	10	2.28
D	20	1.12
E	30	0.76

Using Tooth Contact Analysis (TCA), 251 equally spaced query locations along the contact's semi-major axis calculate the prevailing local load intensity, contact curvature, and rolling and sliding velocities. A complete meshing cycle is simulated using 150 time steps for each scenario in Table 3. The resulting 251-by-150 data arrays form input to the analytical Thermal EHL (TEHL) model.

The size of each discretized cell in the TEHL model was selected through iterative trial-and-error, allowing appropriate compromise between computational effort and any loss of necessary resolution to observe the effects of contact ellipse truncation at the edges of contacting flanks. Consequently, the analytical TEHL model discretises the prevailing contact width (along the semi-major axis) into 128 equally-spaced sampling points. Variations in the

tribological parameters at each discretised location are acquired for a complete meshing cycle, simulated in 100 time-steps.

For the purposes of estimating the instantaneous film thickness (Equation (1)), the contact geometry and kinematics are taken as those at the centre of the instantaneous contact. Figure 4 shows the variation of the central lubricant film thickness, as a pair of teeth meshing contact progresses from the root to the tip.

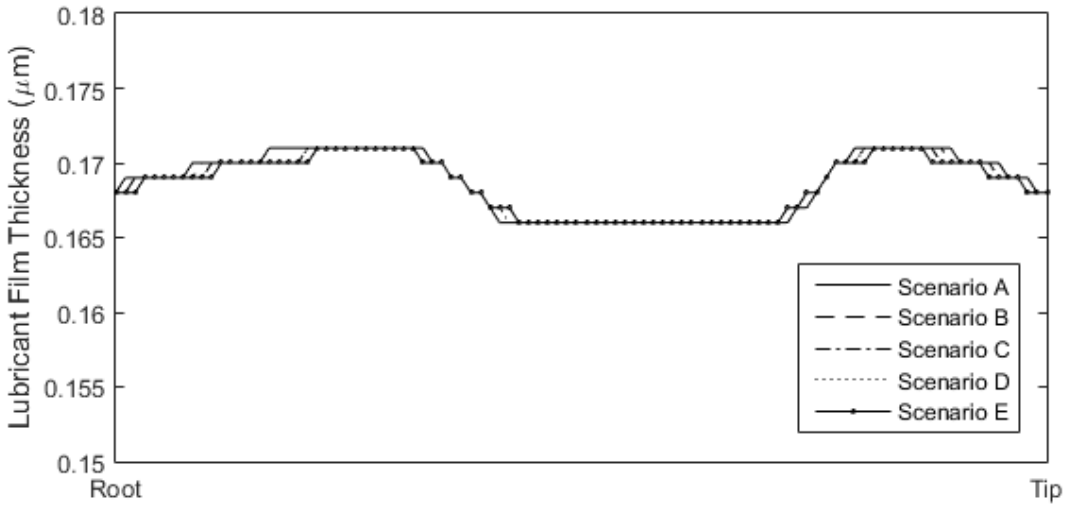

Figure 4: Central lubricant film thickness variation in a meshing cycle

Hereinafter, all figure suffixes correspond to the scenario studied. The vertical axes in Figures 5-7 and 9 have been normalised to represent the length of the active tooth flank in the direction of the tooth profile. Similarly, the horizontal axis represents the length along the flank from one edge to the other (i.e. the lead direction), and is equivalent to the tooth width.

Figures 5a-d show the variation of the contact footprint geometry at seven discrete locations on the active flank, as a single teeth meshing contact progresses from the tooth root to the tooth tip for scenarios A-D under the loading conditions given in Table 1.

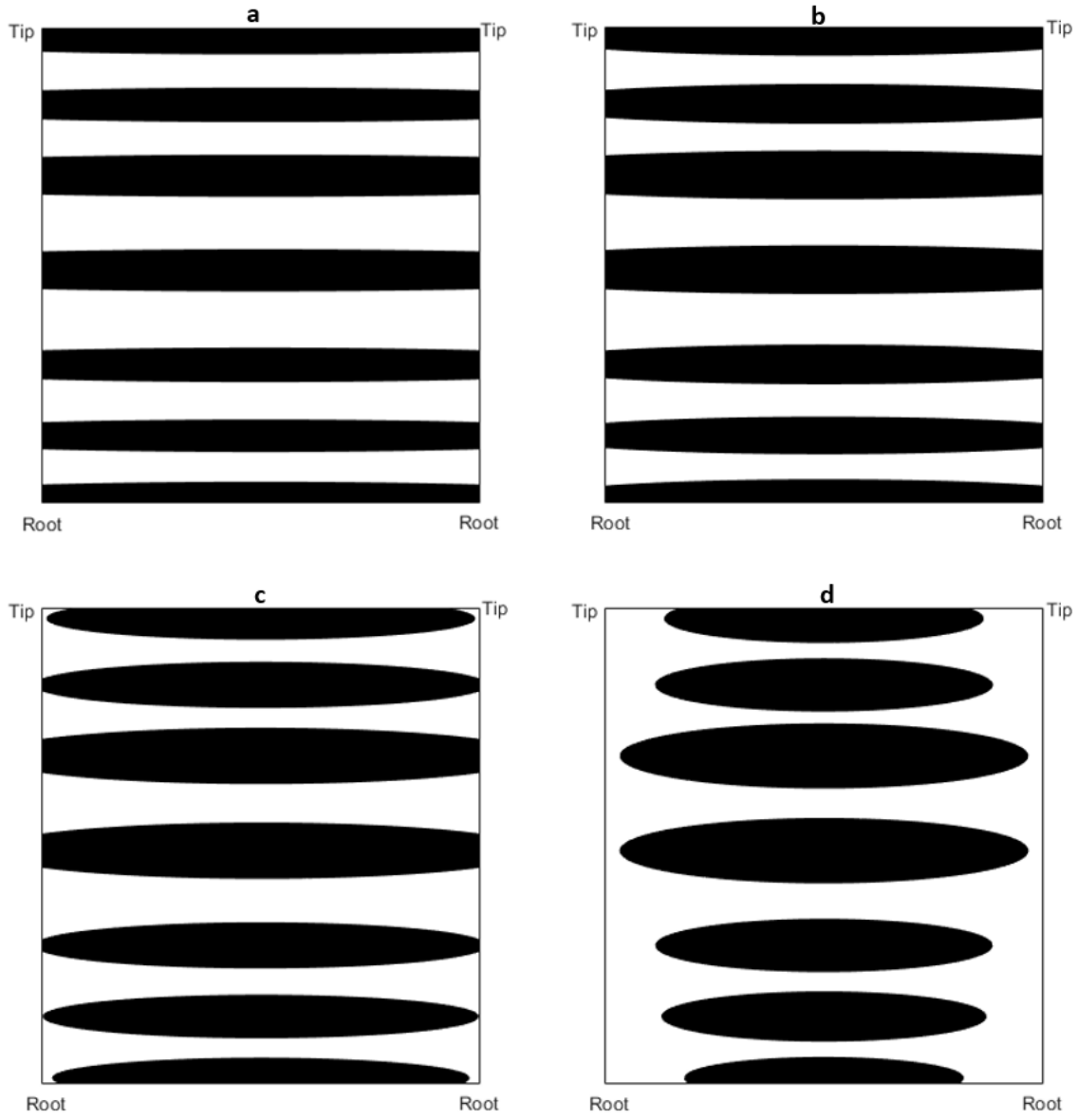

Figure 5: Variation of contact footprint geometry in a meshing cycle for: a) Scenario, A b) Scenario B, c) Scenario C, and d) Scenario D

With sufficient load or small crowning amounts, any crowning induced curvature is flattened. If this semi-major width of the resulting contact ellipse is larger than the available tooth width, the contact footprint is truncated along the edges of the gear flank. This is observed for the total duration of contact from its root to its tip in Figures 5a and 5b. Figure 5c shows truncation only occurs when the contact is approximately half-way up the flank. This is because while the contact on the active flank remains in the vicinity of the flank tip and root, leading and trailing teeth are still in contact with their respective teeth pairs. Thus, the load is shared between them and the individual tooth loads are usually at their lowest values, subject of course to the instantaneous load-share ratio: lf. However, as the meshing contact passes through the central

region of the flank, the load is no longer shared among multiple teeth pairs. It is wholly borne by a single instantaneous contact footprint. As contact truncation occurs, stress discontinuities create pressure concentrations at the edges of the flank. This is observed in Figure 6a and to a lesser extent in Figure 6b.

A crowning magnitude of 10µm (Figure 6c) is found to be sufficient to mitigate pressure concentrations at the contact edges. This is illustrated by the uniform pressure fields on the flank edges in Figure 6c. However, the redistribution of load on the active tooth flank creates areas of significantly higher pressures towards the flank centre, even though the total active flank area remains largely unchanged (Figure 6a-6c). Regions, where contact does not occur are illustrated in black. This trend of increased pressures at the flank centres is further exaggerated in Figure 6d, where the extent of crowning is higher and the active contact area is reduced, as would be expected.

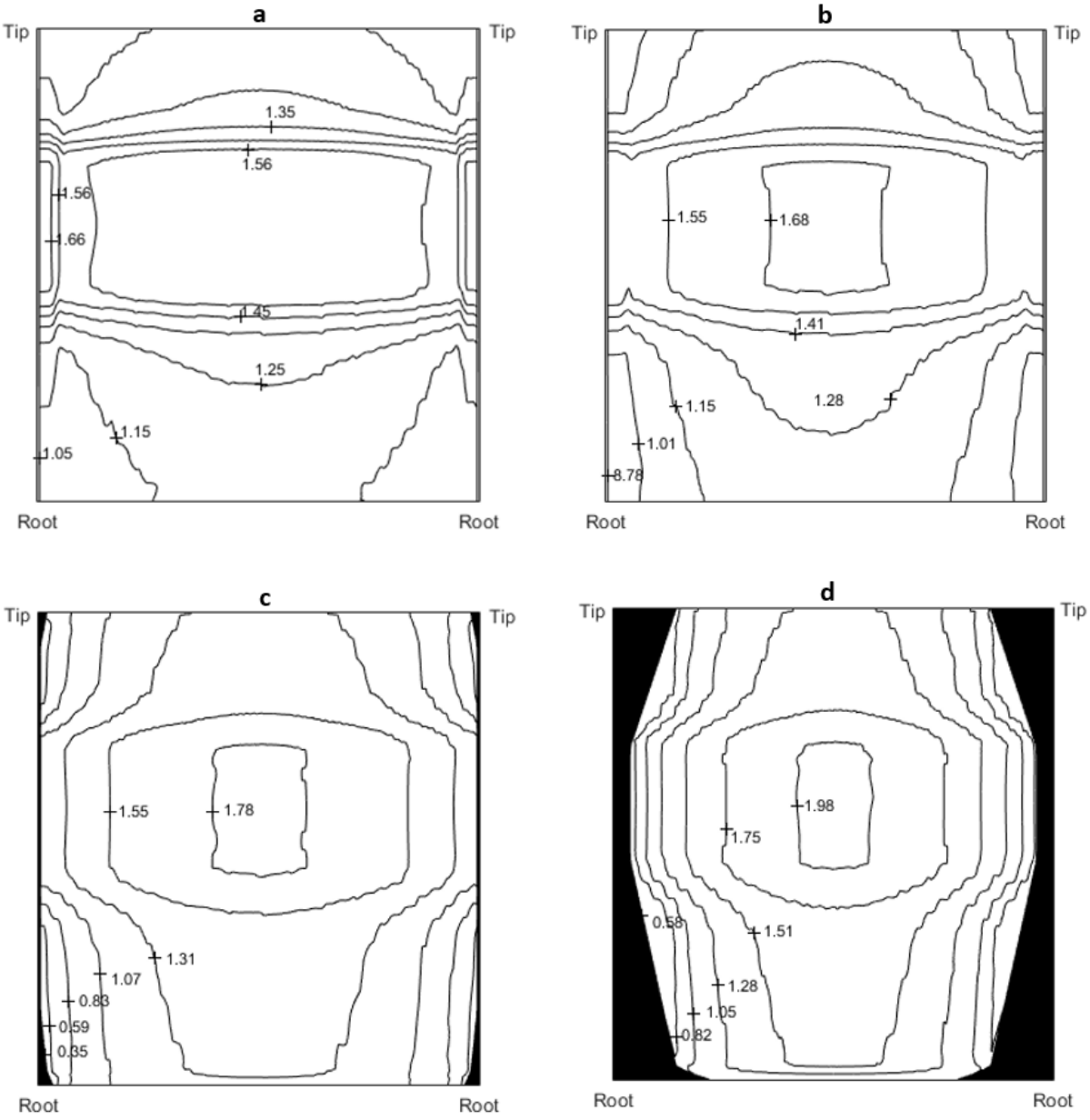

Figure 6: Contact Pressure distribution on active flank (GPa) – complete meshing cycle: a) Scenario A, b) Scenario B, c) Scenario C, and d) Scenario D

While the elimination of the stress discontinuity will undoubtedly carry significant implications in the fatigue wear of the flank edges and lubricant impingement through the side walls of the gear teeth, this study focusses on the resulting effects on power losses

Fig. 7a-7d show the contact power loss per unit length (W/mm), the integral of which along the tooth flank width would yield the total instantaneous power loss. The contact losses are highest at the start and end of the meshing cycle, where the relative sliding velocities between the contacting teeth pair is highest. This corresponds to the tooth root and the tooth tip contact regions respectively. Similarly, power losses are lowest where the gear contact passes through

the pitch point (approximately half-way between the flank root and tip) and the contact experiences pure rolling. This trend is observed in Figures 7a-7d.

The crowning-induced curvature along the semi-major axis of the contact causes slight variations in the local surface geometry and induces some variations in the sliding velocities along the semi-major axis. Though this variation is small, its effects are exaggerated as sliding velocity tends to zero as the meshing contact approaches pitch point. The influence on power losses can be seen as undulations in contours of Figures 7a-7d.

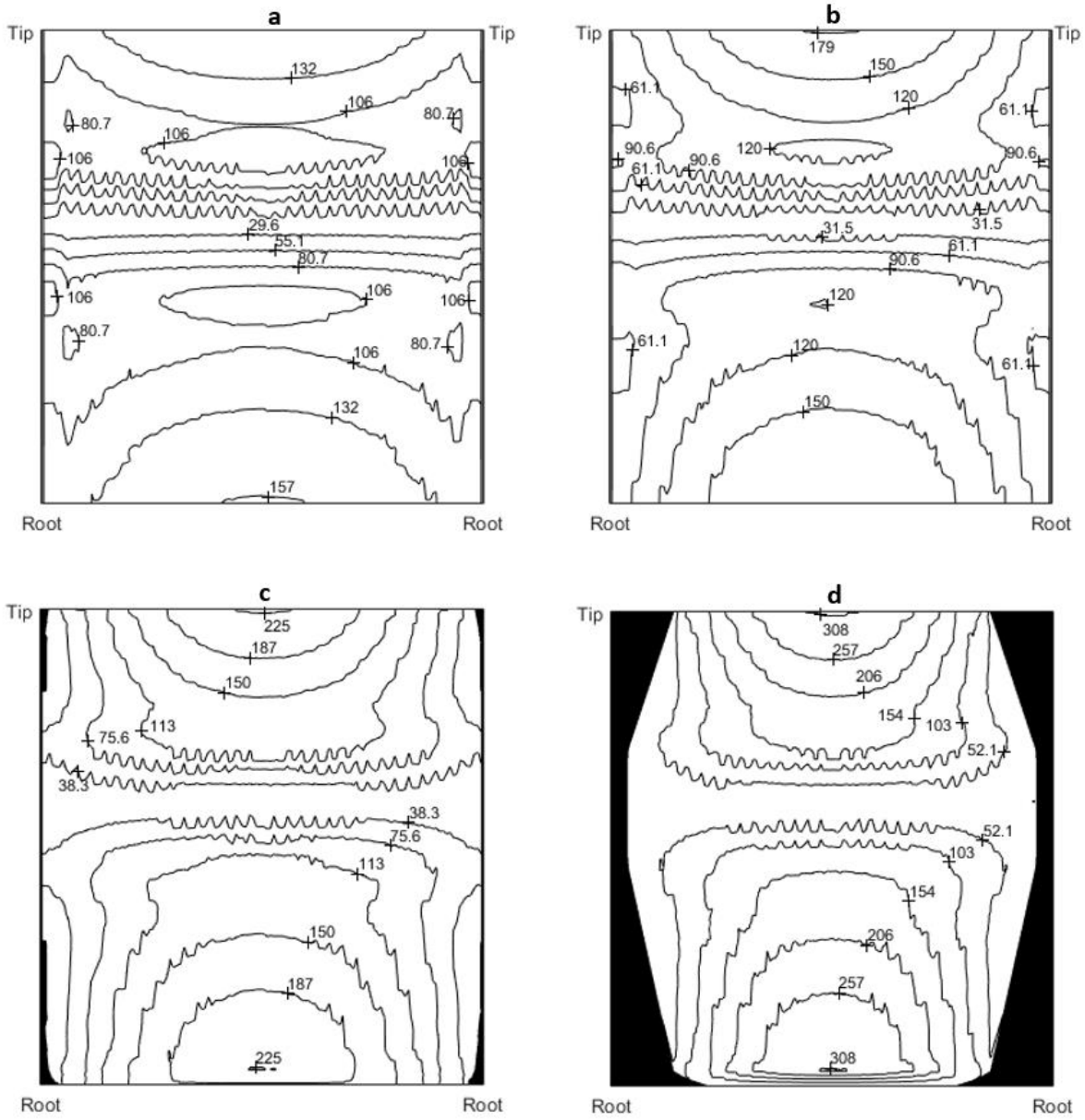

Figure 7: Contact Power loss distribution (W/mm) for a complete meshing cycle: a) Scenario A, b) Scenario B, c) Scenario C, and d) Scenario D

With increasing crowning, Figures 7a-7d show a gradual shift and increase in the contact losses towards the centre of the flank; a consequence of the pattern observed in the pressure isobars of Figures 6a-6d. When contact truncation occurs (Figures 7a-7b), the power losses are higher in the localized regions along the edges of the flank which correlate to the areas of pressure concentrations that result from the aforementioned stress discontinuity. However, even though the active flank area remains largely unchanged as in Figures 7a-7c, the distribution of contact losses is noticeably less severe with lesser crowning. This remains the case when considering the magnitude of the total contact power losses incurred for a complete meshing cycle.

Figure 8 shows a larger percentage and magnitude of contact losses with increasing crowning. While crowning is quite important in mitigating fatigue due to edge loading and thus enhances reliability, this shows how in some cases crowning can have a detrimental effect on efficiency.

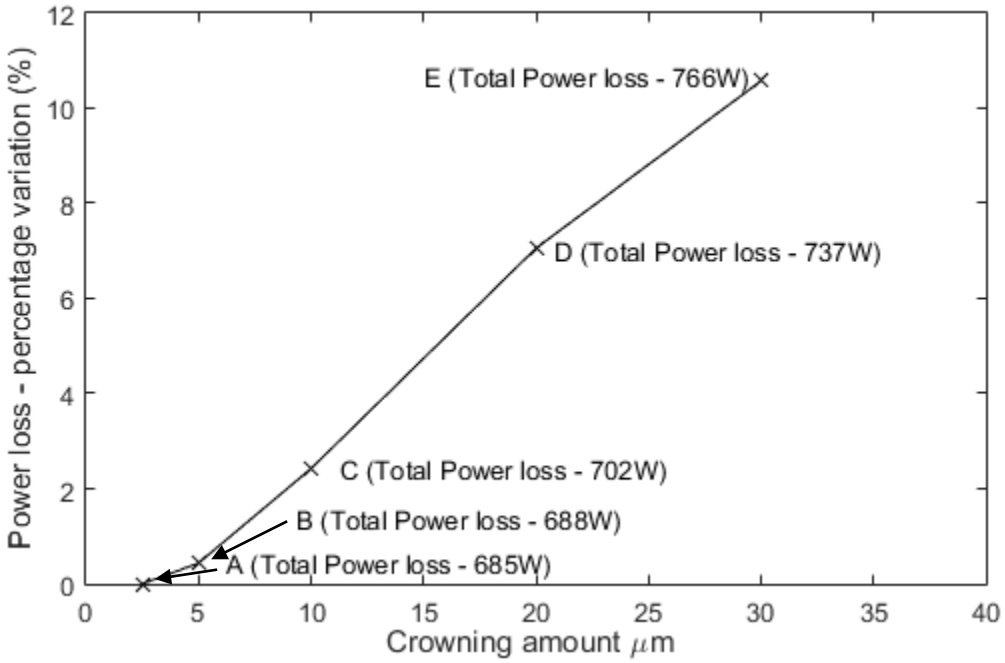

Figure 8: Percentage variation in contact losses relative to Scenario A (‘A’ in figure) – stated values are for a single active flank

Figures 9a-d show the lubricant centreline temperatures in the active flank area. Contact temperatures are highest at the root and at the tip as there is higher relative sliding velocities of the surfaces in these regions. Mid-meshing cycle where the contact is in the region of the flank

centre and sliding velocity is lowest, temperature rise is minimal as temperatures remain closer to bulk temperature of 130°C.

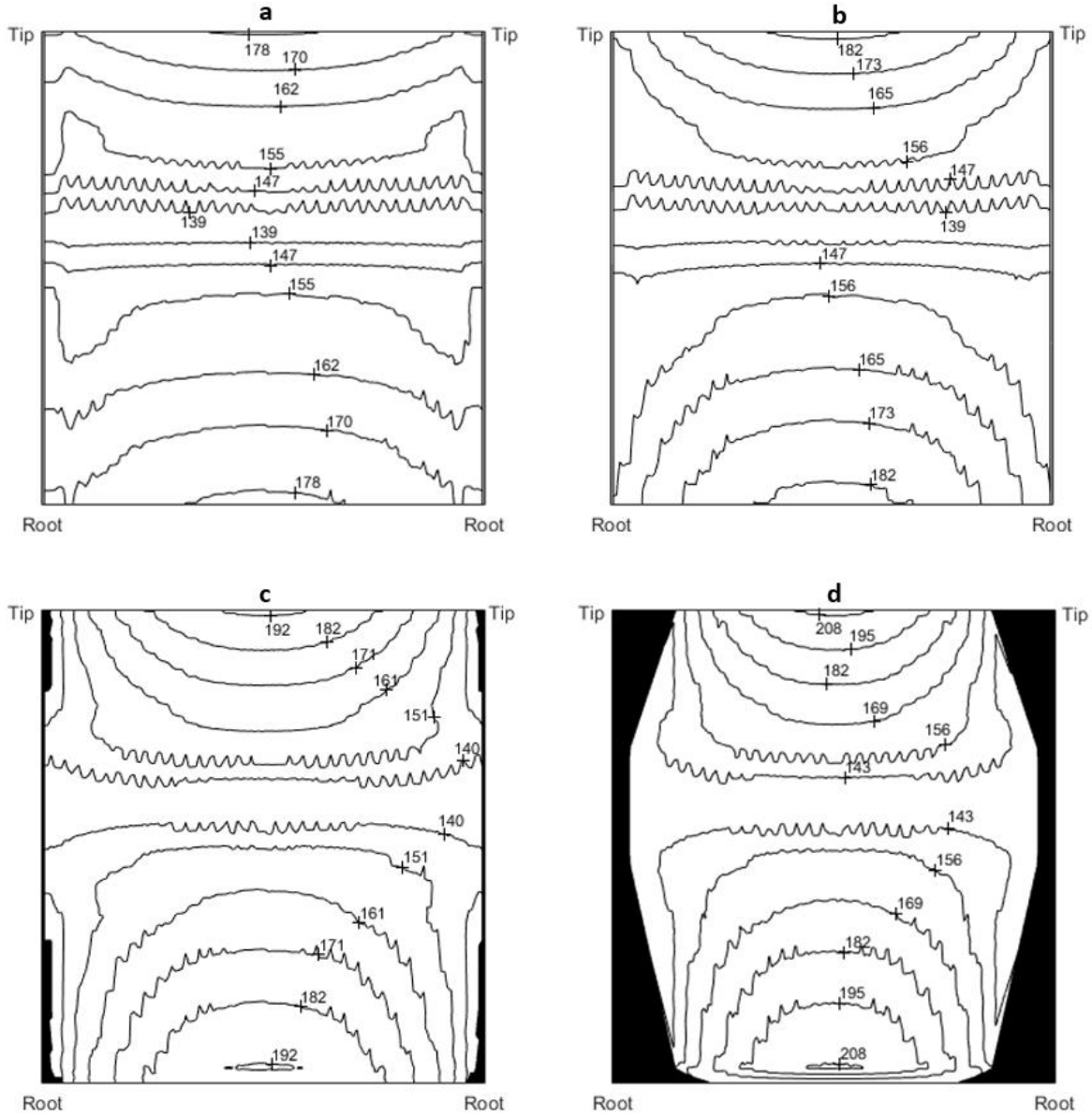

Figure 9 Contact flash temperature distribution (°C) for a complete meshing cycle: a) Scenario A, b) Scenario B, c) Scenario C, and d) Scenario D

With increasing crowning, Figures 9a-9d show a gradual increase in the maximum contact temperatures near the root and the tip of the flank. With contact truncation (Figure 9a), contact temperatures are observably higher in the localized regions along the edges of the flank. Mid-meshing cycle where the contact is in the vicinity of the flank centre, the temperatures at the edges of the flank rise by approximately 8°C more than at the contact centre (Figure 9a). However, this variation becomes less pronounced with a slight increase in crowning, even when truncation and the stress discontinuity is still present (Figure 9b). When crowning

sufficiently mitigates the edge pressure concentrations (Figure 9c), the temperature rises by approximately 15°C more than in the case of Figure 9a even though the active flank area remains largely unchanged. This trend is further pronounced in Figure 9d.

4- Conclusions

The high loading conditions experienced in compact high performance transmissions can cause contact footprint truncation in the meshing gear teeth pairs. This phenomenon causes stress discontinuities and therefore high edge pressures. These pressure concentrations can be detrimental to durability. It can also act to discourage lubricant flow into these regions of the contact when lubricant nozzles are directed onto the side wall of the meshing gears. High pressure spikes have been shown to inhibit lubricant entrainment, resulting in very thin lubricant films in rolling element bearings [4] as well as cam-tappet contacts [35].

Crowning is used primarily as a palliative measure for misalignment issues, which exacerbate the effect of edge pressure spikes. Crowning reduces the magnitude of high pressure spikes at gear flank edges and its associated undesirable repercussions. While the reduction of contact area generally implies lowered contact friction, the redistribution of pressure as the result of crowning can increase the average contact pressures over the contact footprint and can increase the frictional power loss. The effect of starvation and cavitation is not included in the current analysis, both of which would have important repercussions as well.

Thermal analysis has shown that for the gears, lubricant and operating conditions considered in this study, peak contact temperatures rise by approximately 15°C when crowning is introduced to mitigate the reduce edge pressure concentrations.

Nomenclature

A_j	Area of a discretised cell
a	Semi-major half-width of contact ellipse
a_j	Semi-major half-width of a discretised cell j
b	Semi-minor half-width of contact ellipse
b_j	Semi-minor half-width of a discretised cell j
c'	Specific heat capacity of solid surfaces
E'	Reduced elastic modulus of the contact
E_r	Reduced Young's modulus of elasticity
$f_{b,j}$	Boundary friction at a discretised cell j

$f_{v,j}$	Viscous friction at a discretised cell j
h_c	Central lubricant film thickness
K	Lubricant thermal conductivity
K'	Solid thermal conductivity
n	Number of discretised cells along the semi-major axis of the contact footprint
$\bar{p}_j, P_{m,j}$	Mean pressure in a discretised cell j
R'	Reduced radius of a counter-formal contacting pair
R_x	Principal radius of curvature along the semi-minor axis (direction of lubricant entrainment)
R_y	Principal radius of curvature along the semi-major axis (side leakage direction)
T	Traction per unit width of contact
t	Tooth flank width
$U_r, \bar{U}$	Rolling velocity (Speed of lubricant entrainment)
ΔU	Sliding velocity
W	Normal contact load

Greek Letters

α	Lubricant pressure-viscosity coefficient
β	Average asperity tip radius
β_L	Thermal conductivity of lubricant
ε	Slope of the lubricant limiting shear stress-pressure dependence
η_0	Lubricant viscosity at atmospheric pressure
θ_O	Bulk solid temperature
θ_c	Contact centre-plane temperature
θ_s	Solid surface flash temperature
ξ	Asperity density
ρ'	Density of solids
σ	Composite Surface roughness
τ_0	Eyring shear stress
τ_L	Limiting shear stress

Abbreviations

TCA	Tooth Contact Analysis
$TEHL$	Thermal Elastohydrodynamic Lubrication

References

[1]- Menday, M.T., Rahnejat, H. and Ebrahimi, M., “Clonk: an onomatopoeic response in torsional impact of automotive drivelines”, Proc. IMechE, , Part D: J. Automobile Engineering, 1999, 213(4), pp. 349-357.

[2]- Johns, P.M. and Gohar, R., "Roller bearings under radial and eccentric loads", Tribology International, 1981, 14(3), pp. 131-136.

[3]- Mostofi, A. and Gohar, R., "Elastohydrodynamic lubrication of finite line contacts", Trans. ASME, J. lubrication Tech., 1983, 105(4), pp. 598-604.

[4]- Kushwaha, M., Rahnejat, H. and Gohar, R., "Aligned and misaligned contacts of rollers to races in elastohydrodynamic finite line conjunctions", Proc. IMechE, Part C: J. Mech. Eng. Sci., 2002, 216(11), pp. 1051-1070.

[5]- Dudley, D. W., "Dudley's gear handbook", 2nd Edition, McGraw-Hill, U.S.A., New York, 1992.

[6]- Mao, K., "Gear tooth contact analysis and its application in the reduction of fatigue wear", Wear, 2007, 262(11), pp. 1281-1288.

[7]- Simon, V., ''Optimal Tooth Modifications for Spur and Helical Gears'', Trans. ASME, J. Mech. Trans. Auto. Design, 1989, 111, pp. 611–615.

[8]- Harianto, J. and Houser, D.R., "A methodology for obtaining optimum gear tooth micro-topographies for noise and stress minimization over a broad operating torque range.", ASME 2007 Int. Design Eng. Tech. Conf. and Computers and Information in Eng. Conf., ASME, Las Vegas, Nevada, USA, 2007.

[9]- Seol, I. H. and Kim, D. H., "The Kinematics and Dynamic Analysis of Crowned Spur Gear Drive", Comput. Methods Appl. Mech. Eng., 1998, 167, pp. 109–118.

[10]- Karagiannis, I., Theodossiades, S. and Rahnejat, H., "On the dynamics of lubricated hypoid gears", Mechanism and Machine Theory, 2012, 48, 94-120.

[11]- Xu, H. and Kahraman, A., "Prediction of friction-related power losses of hypoid gear pairs", Proc. IMechE, Part K: J. Multi-body Dynamics, 2007, 221(3), pp. 387-400.

[12]- Li, S. and Kahraman A., "A transient mixed elastohydrodynamic lubrication model for spur gear pairs", Trans ASME, J. Tribology, 2010, 132(1), 011501.

[13]- Mohammadpour, M., Theodossiades, S. and Rahnejat, H., "Elastohydrodynamic lubrication of hypoid gear pairs at high loads", Proc. IMechE, Part J: J. Engineering Tribology, 2012, 226(3), pp. 183-198.

[14]- Grubin, A. N., "Contact Stresses in Toothed Gears and Worm Gears", Book 30 CSRI for Technology and Mechanical Engineering, Moscow, DSRI Trans., 1949, No 337.

[15]- Dowson, D. and Higginson, G.R., "A numerical solution to the elastohydrodynamic problem", Proc IMechE., J Mech. Eng. Sci., 1959, 1, pp. 6-15.

[16]- Archard, J.F. and Cowking, E.W., "Elastohydrodynamic lubrication at point contacts", Proc. IMechE, J. Mech. Eng. Sci., 1965, 180(2), pp. 47-56

[17]- Ranger, A.P., Ettles, C.M.M. and Cameron, A., "The solution of point contact EHL problem", Proc. Roy. Soc., Ser. A, 1975, 346 (1645), pp. 227-244.
[18]- Hamrock, B.J. and Dowson, D., "Isothermal elastohydrodynamic lubrication of point contacts, Part II – Ellipticity parameter results", Trans. ASME, J. Lubn. Tech., 1976, 98, pp. 375-383.

[19]- Johns-Rahnejat, P.M., "Pressure and stress distribution under elastohydrodynamic point contacts", Doctoral dissertation, Imperial College of Science and Technology, University of London, 1988.

[20]- Jalali-Vahid, D., Rahnejat, H., Gohar, R. and Jin, Z.M., "Comparison between experiments and numerical solutions for isothermal elastohydrodynamic point contacts", J. Phys., D: Applied Physics, 1998, 31(20):2725.

[21]- Rahnejat, H., "Influence of vibration on the oil film in concentrated contacts", Doctoral dissertation, Imperial College London, University of London, 1984.

[22]- Mostofi, A. and Gohar, R., "Oil film thickness and pressure distribution in elastohydrodynamic point contacts", Proc. IMech, J. Mech. Eng. Sci., 1982, 24(4), pp. 173-182.

[23]- Chittenden, R. J. Dowson, D., Dunn, J. F. and Taylor, C. M., "A theoretical analysis of the isothermal elastohydrodynamic lubrication of concentrated contacts. II. General Case, with lubricant entrainment along either principal axis of the Hertzian contact ellipse or at some intermediate angle", Proc. Roy. Soc., Ser. A, 1985, 397, pp. 271-294.

[24]- Gohar, R. and Rahnejat, H., "Fundamentals of Tribology", Imperial College Press, London, 2008.

[25]- Tipei, N., "Boundary conditions of a viscous flow between surfaces with rolling and sliding motion", Trans. ASME, J. Tribology, 1968, 90(1), pp. 254-261.

[26]- Johns-Rahnejat, P. M., and R. Gohar, "Measuring contact pressure distributions under elastohydrodynamic point contacts", Tribotest, 1994, 1(1), pp. 33-53.

[27]- Mohammadpour, M., Johns-Rahnejat, P.M., Rahnejat, H. and Gohar, R., "Boundary conditions for elastohydrodynamics of circular point contacts", Tribology Letters, 2014, 53(1), pp. 107-118.

[28]- Litvin, F. L, Fuentes, A., Fan, Q. and Handschuh, R. F., "Computerized design, simulation of meshing, and contact and stress analysis of face-milled formate generated spiral bevel gears", Mech. and Mach. Theory, 2002, 37, pp. 441–459

[29]- Evans, C.R. and Johnson, K.L., "Regimes of traction in elastohydrodynamic lubrication", Proc. IMechE, J. Mech. Eng. Sci., 1986, 200(5), pp. 313–324.

[30]- Crook, A. W., "The lubrication of rollers III. A theoretical discussion of friction and the temperatures in the oil film", Phil. Trans. Roy. Soc., A: Math., Phys. and Eng. Sci., 1961, 254 (1040), pp. 237-258.

[31]- Johnson, K. L. and Greenwood, J. A., "Thermal analysis of an Eyring fluid in elastohydrodynamic traction", Wear, 1980, 61(2), pp. 353-374.

[32]- Greenwood, J.A. and Tripp, J.H., "The contact of two nominally flat rough surfaces," Proc. IMechE, J. Mech. Eng. Sci., 1970, 185, pp. 625–633.

[33]- Teodorescu, M., Balakrishnan, S. and Rahnejat, H., "Integrated tribological analysis within a multi-physics approach to system dynamics", Tribology and Interface Engineering Series 48, 2005, pp. 725-737.

[34]- Briscoe, B. J. and Evans, D. C. B., "The shear properties of Langmuir-Blodgett layers", Proc. Roy. Soc., Ser. A: Math., Phys. and Eng. Sci., 1982, 380(1779), pp. 389-407.

[35]- Kushwaha, M. and Rahnejat, H., "Transient elastohydrodynamic lubrication of finite line conjunction of cam to follower concentrated contact", J. Phys., D: Applied Physics, 2002, 35(21):2872.